Science of The Total Environment
May 2020, Volume 715 Pages 136834 (13p.)
https://doi.org/10.1016/j.scitotenv.2020.136834
https://archimer.ifremer.fr/doc/00606/71802/

Intraspecific variability in membrane proteome, cell growth, and morphometry of the invasive marine neurotoxic dinoflagellate *Alexandrium pacificum* grown in metal-contaminated conditions

Chetouhi Cherif [1], Masseret Estelle [2], Satta Cecilia Teodora [3], Balliau Thierry [4], Laabir Mohamed [2], Jean Natacha [1, *]

[1] Mediterranean Institute of Oceanography, Equipe Microbiologie Environnementale et Biotechnologie, UM 110 CNRS/IRD Aix-Marseille Université, Université de Toulon, CS 60584, 83 041 Toulon Cedex 9, France
[2] Marbec, University of Montpellier, IRD, Ifremer, CNRS, 34 095 Montpellier Cedex 5, France
[3] University of Sassari, via Piandanna 4, Agenzia Regionale per la Ricerca in Agricoltura, Loc. Bonassai, Olmedo, 07 100 Sassari, Italy
[4] PAPPSO-GQE-Le Moulon, INRA, Université Paris-Sud, CNRS, AgroParisTech, Université Paris-Saclay, 91 190 Gif-sur-Yvette, France

* Corresponding author : Natacha Jean, email address : jean@univ-tln.fr

Abstract :

Over the past decades, the occurrence, distribution and intensity of harmful algal blooms involving the dinoflagellate Alexandrium pacificum have increased in marine coastal areas disturbed by anthropogenic inputs. This invasive species produces saxitoxin, which causes the paralytic shellfish poisoning syndrome in humans upon consumption of contaminated seafood. Blooms of A. pacificum have been reported in metal-contaminated coastal ecosystems, suggesting some ability of these microorganisms to adapt to and/or resist in metal stress conditions. This study seeks to characterize the modifications in membrane proteomes (by 2-D electrophoresis coupled to LC-MS/MS), cell growth and morphometry (measured with an inverted microscope), in response to metal stress (addition of Zn2+, Pb2+, Cu2+ and Cd2+), in two Mediterranean A. pacificum strains: SG C10-3 and TAR C5-4F, respectively isolated from the Santa Giusta Lagoon (Sardinia, Italy) and from the Tarragona seaport (Spain), both metal-contaminated ecosystems. In the SG C10-3 cultures grown in a metal cocktail, cell growth was significantly delayed, and cell size increased (22% of 37.5 µm cells after 25 days of growth). Conversely, no substantial change was observed for cell growth or cell size in the TAR C5-4F cultures grown in a metal cocktail ($P > 0.10$), thus indicating intraspecific variability in the responses of A. pacificum strains to metal contamination. Regardless of the conditions tested, the total number of proteins constituting the membrane proteome was significantly higher for TAR C5-4F than for SG C10-3, which may help TAR C5-4F to thrive better in contaminated conditions. For both strains, the total number of proteins constituting the membrane proteomes was significantly lower in response to metal stress (29% decrease in the SG C10-3 proteome: 82 ± 12 proteins for controls, and 58 ± 12 in metal-contaminated cultures; 17% decrease in the TAR C5-4F proteome: 101 ± 8 proteins for controls, and 84 ± 5 in metal-contaminated cultures). Moreover, regardless of the strain, proteins with significantly modified expression in response to stress were mainly

down-regulated (representing 45% of the proteome for SG C10-3 and 38% for TAR C5-4F), clearly showing the harmful effects of the metals. Protein down-regulation may affect cell transport (actin and phospholipid scramblase in SG C10-3), photosynthesis (RUBISCO in SG C10-3, light-harvesting protein in TAR C5-4F, and high-CO2-inducing periplasmic protein in both strains), and finally energy metabolism (ATP synthase in both strains). However, other modifications in protein expression may confer to these A. pacificum strains a capacity for adaptation and/or resistance to metal stress conditions, for example by (i) limiting the metal entry through the plasma membrane of the SG C10-3 cells (via the down-regulation of scramblase) and/or (ii) reducing the oxidative stress generated by metals in SG C10-3 and TAR C5-4F cells (due to down-regulation of ATP-synthase).

Graphical abstract

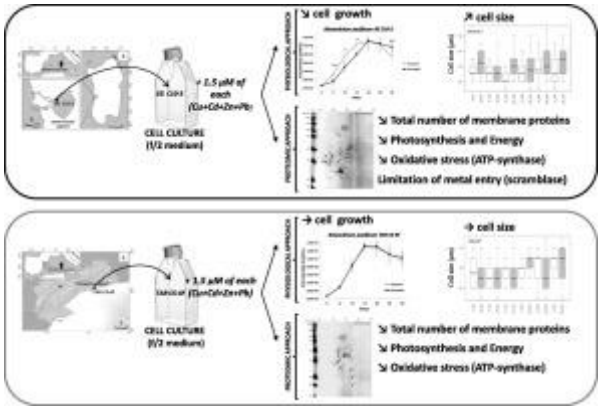

Highlights

► Growth inhibited under metal stress for *A. pacificum* SG C10-3, not for TAR C5-4F. ► SG C10-3 shows increased cell sizes under metal stress, not TAR C5-4F. ► Metals down-regulate proteins, decrease the number of proteins in the proteomes. ► Protein down-regulation affects photosynthesis/energy metabolism in both strains. ► Proteomic modifications promote cell adaptation in metal-contaminated ecosystems.

Keywords : Alexandrium pacificum, harmful algal bloom, proteomics, membrane proteome, trace metals

INTRODUCTION

Among the dinoflagellates involved in harmful algal blooms (HABs), the genus *Alexandrium* causes HABs that induce the paralytic shellfish poisoning (PSP), due to its production of saxitoxin and derivates (Anderson et al., 2012). Saxitoxins cause human neural system syndromes with approximately 2 000 cases of toxicity per year worldwide (Quod and Turquet, 1996), lead to mass mortalities of fish, shellfish, marine mammals, and birds (Hallegraeff, 1993), and trigger severe economic impacts on aquafarming (Hoagland et al., 2002; Park et al., 2013).

The species *Alexandrium pacificum* Litaker (ex *A. catenella* (Whedon and Kofoid), Balech) is widely distributed throughout the world, observed along Mediterranean, Pacific, and Antarctic coasts (Vila et al., 2001; Masseret et al., 2009; John et al., 2014). In the Mediterranean area, proliferations of *A. pacificum* can occur in marine areas contaminated with trace metals, such as the Tyrrhenian coasts (Italy), the Balearic and Catalan coasts, the Thau Lagoon (France), the Bizerte Lagoon (Tunisia) (Penna et al., 2005, Bravo et al., 2008, Laabir et al., 2013,

Fertouna-Bellakhal et al., 2015), and *Alexandrium* spp. have been observed in Toulon Bay (western Mediterranean, France), where the water column and sediments are severely metal-contaminated (Jean et al., 2005; Tessier et al., 2011; Jean et al., 2012). Occurrences of *A. pacificum* in such areas suggest that it can adapt and/or is resistant to metal contamination. To date, much effort has been devoted to understanding *A. pacificum* physiology, *via* the study of toxin biosynthesis (Wang et al., 2006; Zhang et al., 2017), mechanisms underlying cell growth (Hadjadji et al., 2014), and the impact of diverse nutrient and environmental conditions on cells (Uribe and Espejo, 2003; Yoo and Shin, 2004; Jauzein et al., 2008; Laabir et al., 2011; Herzi et al., 2013). However, few studies have investigated the possible ability of this dinoflagellate to adapt and/or resist in disturbed environments, such as metal-contaminated marine coastal ecosystems. Thus, studies characterizing the possible tolerance and/or resistance of *A. pacificum* to metal stress are needed to better understand its potential capacity to develop in certain metal-polluted marine environments.

"Omics" approaches provide insight into the responses and the adaptation mechanisms developed by organisms exposed to environmental stresses (Jean et al., 2012). Proteomic approaches have revealed an intraspecific variability between a toxicity-lost mutant and the wild-type of *A. pacificum*, through differentially expressed proteins involved in its toxicity (Zhang et al., 2015). The proteome involved in the various toxin biosynthesis stages by *A. pacificum* has been characterized (Wang et al., 2013). An ecotoxicoproteomic study on the Mediterranean strain (ACT03) of *A. pacificum* showed that single-stress by lead or zinc induced the down-regulation of many proteins constituting its soluble proteome, compensated by the up-regulation of some proteins like ATP-synthase able to contribute to an adaptive proteomic response in metal-contaminated ecosystems (Jean et al., 2017). Using an *in silico* approach, the secretome of *A. pacificum* has been predicted, showing that 47% of the secreted proteins are enzymes (peptidases) active in the extracellular medium during stress responses,

which could help this dinoflagellate to develop in various environmental conditions, such as in metal-contaminated areas (Chetouhi et al., 2019).

The plasma membrane, the first barrier against biotic or abiotic stresses in all organisms, mediates the exchange of molecular information between the intracellular and the extracellular environment. Biomolecules located in this membrane play important roles in stress signal transduction. Some studies have reported that the plasma membrane is involved in a variety of mechanisms for metal detoxification and tolerance, for example, by (*i*) reducing metal uptake, (*ii*) stimulating the efflux pumping of metals that have entered the cytosol, (*iii*) repairing metal stress- damaged proteins, (*iv*) chelating metals and/or (*v*) compartmenting metals away from metabolic processes by transport into the vacuole (Hall, 2002). Consequently, the study of the effects of metal stress on the proteins constituting the *A. pacificum* membrane proteome will help understand how metals affect plasma membrane proteins, by degrading them and/or down- or up-regulating their expression, and as a result, by inducing a modified protein expression that can lead to cell-resistance mechanisms and adaptation in *A. pacificum*.

Investigations about changes in the proteome during the cell cycle of *Prorocentrum triestinum* showed strong relationships between its protein expression and its cell cycle (Chan et al. 2004). The growth cycle controls the DNA cycle which is mediated by proteins necessary for the DNA replication (Alberghina and Sturani, 1981). Besides, there is a relationship between cell division and cell size during cell growth, some studies reporting that delays in cell division, due to increased interdivision time, lead to higher cell sizes (Vadia and Levin, 2015). Multiple effects of the metal stress are expected simultaneously on the proteomes, the cell growth and the cell sizes of *A. pacificum*.

As a result, the present study combines ecotoxicoproteomic and physiological approaches to compare the responses to a multiple-metal stress in two different strains of *A. pacificum*,

coming from two metal-contaminated Mediterranean areas: the SG C10-3 strain isolated from the Santa Giusta Lagoon (Luglié et al., 2002), and the TAR C5-4F strain from the Tarragona seaport (Bravo et al., 2008). The main objectives of this study were to (*i*) evaluate the extent physiological variations in *A. pacificum* cells by following their density and morphometry during growth in the presence of metals (*ii*) determine the changes in the plasma membrane proteome induced by metal stress. Based on these results, we built a model to depict how certain strains of *A. pacificum* react and could improve their resistance to metals in disturbed marine ecosystems.

MATERIAL AND METHODS

1. Alexandrium pacificum cultures, growth kinetics and morphometry

1.1. Strains

The two studied strains of *Alexandrium pacificum* were obtained from germination of single cysts isolated from sediments collected in respectively the Santa Giusta Lagoon (Sardinia, Italy) for the SG C10-3 strain and in the Tarragona seaport (Spain) for the TAR C5-4F strain (**Figure 1**). In the Santa Giusta Lagoon, contamination by diverse trace metals has been reported in the surface sediments of the lagoon (for example: Zn^{2+}=47.6 µg g^{-1}, Pb^{2+}=9.9 µg g^{-1}, Cu^{2+}=9.6 µg g^{-1}, and Cd^{2+}=3.8 µg g^{-1}) (Luglié et al., 2002). Similarly, the shallow sediments of the Tarragona seaport, an area of intense shipping traffic that receives discharges from major rivers, are contaminated by various trace metals (for example: Zn^{2+}=45.0 µg g^{-1}, Pb^{2+}=19.9 µg g^{-1}, Cu^{2+}=12.1 µg g^{-1}, and Cd^{2+}=0.6 µg g^{-1}) (Bravo et al., 2008; Pinedo et al., 2014).

1.2. Cultures

The obtained monoclonal cultures were maintained in f/2 culture medium (*i.e.* containing: $NaNO_3$, NaH_2PO_4, Na_2EDTA, $FeCl_3$, $ZnSO_4$, $CoSO_4$, $MnSO_4$, Na_2MoO_4, Na_2SeO_3, $NiCl_2$, thiamine HCl, biotin, cyanocobalamin) (Guillard and Ryther, 1962), at 20°C in sterile 250 mL flasks (75 cm^2 Greiner, Dominique Dutscher SAS), under light intensity of 135 µmol photons m^{-2} s^{-1}, with a photoperiod of 12 h:12 h (light:dark) (Herzi et al., 2013, 2014). Natural seawater, filtered through a GF/F grade glass fiber filter (Ø= 47 mm, Whatman) and then sterilized, was used for the culture medium.

To study the variations in cell growth, morphometry, and membrane proteomes in *A. pacificum* cultures exposed to metal stress, the f/2 medium was supplemented with a cocktail of sterile stock solutions of metals, prepared with $ZnSO_4,7H_2O$, $Pb(CH_3COO)_2,3H_2O$, $CuSO_4,2H_2O$ or $3CdSO_4,8H_2O$ salts (chosen for their solubility) dissolved in ultrapure water, to reach a total concentration of 1.5 µM for each metal (Zn^{2+}, Pb^{2+}, Cu^{2+} and Cd^{2+}), giving a total metal concentration (M_T^{2+}) of 6 µM in the obtained metal cocktail culture medium. A metal-free culture medium was used as the control (**Figure 2A**). Trace metals used in this study have been chosen since they contamine in general marine metal-contaminated coastal ecosystems: Zn^{2+} and Cu^{2+} are essential for cells as oligo-elements but toxic at high levels, whereas Pb^{2+} and Cd^{2+} are always toxic for the cells (Tessier et al., 2011; Jean et al., 2012). Based on the MINEQL-program (Garnier et al., 2004) and on the known composition of the f/2 medium, the estimated corresponding free metal concentrations (M_F^{2+}) bioavailable for toxicity towards cells were then calculated (Herzi et al., 2013, 2014): $Zn_F^{2+}= 0.67\times10^{-7}$ M, $Pb_F^{2+}= 2.56\times10^{-9}$ M, $Cu_F^{2+}= 4.96\times10^{-10}$ M and $Cd_F^{2+}= 0.70\times10^{-8}$ M. These used concentrations have been chosen similar in units to those directly measured in marine metal-contaminated coastal ecosystems (Tessier et al., 2011; Jean et al., 2012). Three independent biological replicates of the SG C10-3 and TAR C5-4F *A. pacificum* cultures were achieved in

control and cocktail conditions, in order to measure their respective cell sizes and growth kinetics.

1.3. Morphometric measurements

The effects of trace metals used in cocktail on morphometry were evaluated by measuring cell sizes (in diameter) in three independent biological replicates of the SG C10-3 and TAR C5-4F *A. pacificum* cultures. These measurements were carried out with an inverted microscope at a magnification of 100×, during the 30 days of their growth (**Figure 2B**). At each point of growth (5 day intervals), the sizes of 50 cells chosen randomly were thus measured for both strains in each condition (control and cocktail).

1.4. Growth kinetics measurements

The effects of trace metals on the growth kinetics were evaluated by counting all the cells present in 30 µL subsample of 1 mL Lugol-fixed culture sample during the growth (every 5 days), with an optical microscope at a magnification of ×40, so as to obtain the density in number of cells per liter of culture (cells L^{-1}) (**Figure 2B**). These measurements were performed on three independent biological replicates of the SG C10-3 and TAR C5-4F *A. pacificum* cultures.

1.5. Statistical analysis

Student's *t*-tests were used to compare the means in cell densities and in cell sizes measured in the three independent biological replicates of the SG C10-3 and TAR C5-4F *A. pacificum* cultures, in control and cocktail conditions (Shapiro-Wilk's test showed that the data followed a normal distribution: $P > 0.05$).

2. Proteomics analysis and protein identification using mass spectrometry

Proteomics analysis and protein identification were carried out on three independent biological replicates of the SG C10-3 and TAR C5-4F *A. pacificum* cultures, obtained in control or cocktail conditions, at the end of exponential phase-early stationary phase of their growth (after 15 days of growth). Cell density was then calculated to ensure that each culture sample studied contained 8×10^6 cells.

2.1. Preparation of protein extracts

The culture samples were centrifuged for 15 min at 1 500 g, at 15°C. The obtained cell pellet was washed twice with sterile filtered natural seawater for 10 min at 15 000 g (Wang et al., 2008). The pellet was then re-suspended in an extraction solution containing 2 mL of 40 mM Tris at pH 8.7, 2.4 µL benzonase nuclease (Sigma-Aldrich) and 10 µL of protease inhibitor cocktail (Sigma-Aldrich) (**Figure 2C**). The obtained suspension was sonicated in ice-water bath, using a microtip Vibra Cell 734 24 (Bioblock Scientific) for 3 min (10s on and 10s off cycles) at 50 W and 25 kHz. Then, the solution was centrifuged for 30 min at 15 000 g. From the pellet containing membrane proteins, 50 mg were used for the membrane protein extraction using the Ready Prep™Protein Extraction Kit Membrane I (Bio-Rad). This kit is based on the separation of membrane proteins with the X-114 detergent (Bordier, 1981; Santoni et al., 2000). The extracted sample was then cleaned using the Kit Ready Prep™ 2D Cleanup (Bio-Rad), which facilitated the preparation of low conductivity samples, suitable for isoelectric focusing (IEF) and SDS-PAGE, during 2-D gel electrophoresis.

2.2. Protein determination

Protein determination of the extracts was achieved using the Reagent Compatible Detergent Compatible Protein Assay (RC DC Protein Assay, Bio-Rad) based on the Lowry method (Lowry et al., 1951), with bovine serum albumin (BSA) as standard.

2.3. 2-D electrophoresis

2-D electrophoresis was performed using 350 µL of extract containing 200 µg of membrane proteins loaded under a pre-prepared immobilized pH gradient (IPG) strip (17 cm length, linear gradient, pH 3–10, Bio-Rad) (Linares et al., 2016) (**Figure 2C**). Rehydration, and then, isoelectric focusing (IEF) of the extract within the IPG strip, was performed in a PROTEAN IEF Cell (Bio-Rad) horizontal electrophoresis system at 20°C. The program used was: 18 h at 50 V (active rehydration), 2 h at 100 V, 2 h at 250 V, 2 h at 500 V, 2 h at 1 000 V, 2 h at 4 000 V and 5 h at 10 000 V, to reach 60 000 Vh for each loaded IPG strip. At the end of IEF, the equilibration of each IPG strip was performed for 10 min at room temperature, in equilibration buffer 1 (6 M urea, 2% w/v SDS, 0.375 M Tris pH 8.8, 20% v/v glycerol and 2% w/v DTT) and buffer 2 (6 M urea, 2% w/v SDS, 0.375 M Tris pH 8.8, 20% v/v glycerol and 2.5% w/v iodoacetamide). The proteins separated by IEF underwent SDS-PAGE (Laemmli, 1970) in 18-cm 12% polyacrylamide gels on the top of which the strip was positioned and sealed with 0.7% agarose. A volume of 20 µL of molecular weight marker solution (10–250 kDa range, Precision Plus Protein Standards Dual Color, Bio-Rad) was loaded at the left top of the gel. The gels were run at 4°C in a Protean II XL (Bio-Rad), with a constant current of 20 mA per gel for 1 h, and then, with a constant current of 30 mA per gel until the dye reached the bottom of the gel. At the end of SDS-PAGE, gels were washed three times for 5 min in ultrapure water, stained with the Imperial Protein Stain (Thermo Fisher Scientific) under orbital shaking for 1.5 h. The gels were then destained in ultrapure water

until visualization of separated protein spots. Each gel presented is representative of three different biological gel replicates. The protein spots on the gels were analyzed using PD Quest 2-D Analysis Software 8.0.1 (Bio-Rad). Abundance of a given protein spot was obtained after normalization, based on the *ratio* (in %) of its individual abundance to the abundance of all the standard marker bands.

2.4. Tracking of proteins of interest

Proteins of interest showed significantly modified expression in response to metal stress, either by up-regulation (or appearance) of protein spots on the contaminated 2-D gels, relatively to those of controls, or by down-regulation (or disappearance) of protein spots on the control 2-D gels, relatively to those obtained in metal stress conditions (Jean et al., 2017). As a result, presence/absence of these proteins corresponded to spots respectively appearing/ disappearing on at least two of the three gel replicates obtained in metal stress conditions, in comparison with controls. To be considered as up-regulated, a protein showed a *ratio* ≥ 2 of the normalized abundance of its spot on the contaminated 2-D gels to the normalized abundance of its spot on the control 2-D gels (Bae et al., 2003). Similarly, a down-regulated protein had a *ratio* ≥ 2 of its normalized abundance of its spot on the control 2-D gels to the normalized abundance of this spot on the contaminated 2-D gels. Then, a Student's *t*-test, comparing the normalized abundances obtained for these protein candidates, in control and in metal-contaminated conditions, was applied to determine if the differences in abundances observed between each condition were significant (highly significant: $P^{***} \leq 0.01$; significant: $0.01 < P^{**} \leq 0.05$; nearly significant: $0.05 < P^{*} \leq 0.10$), in which case the corresponding proteins were considered as proteins of interest (up- or down-regulated).

2.5. Protein identification using liquid chromatography-tandem mass spectrometry

To identify the proteins of interest by liquid chromatography-tandem mass spectrometry (LC-MS/MS) (**Figure 2C**), the corresponding protein spots were excised from gels. The digestion of proteins was performed according to a standard trypsin protocol (Aloui et al., 2018). Ultimate 3000 RSLC nano system (Thermo Scientific) was used for HPLC. 4 µL of solution contained peptide sample was loaded at 30 µL min^{-1} on a precolumn cartridge (stationary phase: C18 PepMap, 5 µm; column: 300 µm inner diameter, 5 mm; Thermo Scientific) and desalted with 0.08% trifluoroacetic acid and 2% acetonitrile (ACN) in water. Then, 3 min later, the precolumn cartridge was connected to the separating PepMap C18 column (stationary phase: C18 PepMap, 3 µm; column: 75 µm inner diameter, 150 mm; Thermo Scientific). The buffer A was prepared with 0.1% HCOOH and 3% ACN in water, and buffer B with 0.1% HCOOH and 80% ACN in water. The peptides were separated with a linear gradient from 4 to 39% B for 14 min at µL min^{-1}. Including the regeneration step at 99% B and the equilibration step at 4% A, one run took 22 min. LTQ Orbitrap Discovery (Thermo Electron) was used to analyze the eluted peptides by nanoelectrospray interface. Liquid junction and a non-coated capillary probe (10 µm inner diameter; New Objective) were used for ionization (1.4 kV ionization potential). Then, peptide ions were analyzed using Xcalibur 2.5.5 SP1 with the following data-dependent acquisition steps: (1) full MS scan (mass-to-charge *ratio* (*m*/*z*) 300-1 400, centroid mode in orbitrap) and (2) MS/MS (qz = 0.22, activation time = 50 ms, and collision energy = 35%; centroid mode in linear trap). Step 2 was repeated for the three major ions detected in step 1. Dynamic exclusion was set to 30 s. Database searches were achieved using X!Tandem (Craig and Beavis, 2004). For protein identification, the *A. pacificum* database of Zhang et al. (2014) (11 437 entries) and a common contaminant database (keratins, trypsin, etc: 55 entries) were used. Protein identification was parsed/validated using the X!TandemPipeline tool, when at least two peptides (at 0.05 E-

value), originating from a single protein (at 0.001 E-value), were significant (Langella et al., 2017). All the proteins constituting the membrane proteomes could not be identified, when: (*i*) corresponding spots were too small (thus impossible to excise in the gels), (*ii*) proteins could not be sequenced for other technical reasons, (*iii*) corresponding protein sequences remained unknown (or hypothetical) in the proteomic databases.

RESULTS

1. *Effects of metal stress on cell growth/morphometry of Alexandrium pacificum strains*

1.1. Effects on cell growth

For the SG C10-3 strain, the initial cell density was systematically 0.77×10^6 cells L^{-1} in the metal-contaminated and control cultures (**Figure 3**). During the exponential phase (days 5, 10, and 15), cell growth slowed down in the metal-contaminated cultures, with cell densities becoming significantly lower than in controls ($0.01 < P \leq 0.10$) (**Table 1 and Supp data 1**). Under metal stress, cell densities were 2.0 fold lower on day 5, 1.5 fold lower on day 10 and 1.3 fold lower on day 15. After the exponential phase (on days 20 and 25), cell growth ultimately reached that of controls, with no significant difference ($P > 0.10$) in cell densities between metal-contaminated and control cultures.

For the TAR C5-4F strain, the initial cell density was systematically 0.65×10^6 cells L^{-1} in the metal-contaminated and control cultures (**Figure 3**). Cell growth of TAR C5-4F in metal-contaminated conditions showed no significant difference from that of controls ($P > 0.10$), whatever the day of growth (**Table 1 and Supp data 1**).

1.2. Effects on the morphometry

Regardless of the *A. pacificum* strain, cell size (in diameter) ranged between 22.5 and 37.5 µm (**Figure 4A**). Boxplots of the morphometric data obtained for the SG C10-3 strain during its cell growth, show that the median cell sizes in metal-contaminated cultures were generally higher than those measured for controls (13% higher on day 5, 20% on day 15, and 18% on day 30) (**Figure 4B**), with significantly higher cell sizes ($P < 0.10$) for cells under metal stress (**Table 1 and Supp data 2**). The proportion of cells at the different sizes (22.5, 25.0, 27.5, 30.0, 32.5, 35.0 and 37.5 µm) revealed that, in metal-contaminated conditions, there was a non-negligible proportion of larger cells (37.5 µm) in the SG C10-3 cultures, from day 5 until the end of the cell growth (10% of 37.5 µm cells on day 20; 22% of 37.5 µm cells on day 25; 16% of 37.5 µm cells on day 30) (**Figure 4C**). By contrast, in the SG C10-3 control cultures, such large cells were observed only at the end of cell growth, and moreover, in much lower proportions (2% of 37.5 µm cells on day 25; 4% of 37.5 µm cells on day 30).

The boxplots of the morphometric data obtained for the TAR C5-4F strain show that median cell sizes were often lower in cultures exposed to metal stress (8% lower on day 15, and 17% on day 25) (**Figure 4B**), with significantly lower cell sizes ($P < 0.10$) on day 15 and day 25 in contaminated conditions (**Table 1 and Supp data 2**). Low proportions of larger cells (37.5 µm) were only observed at the end of the growth in metal-contaminated TAR C5-4F cultures (2% of 37.5 µm cells on day 20; 4% of 37.5 µm cells on day 25; 18% of 37.5 µm cells on day 30), whereas such large cells were observed in TAR C5-4F control cultures on day 30 (8% of 37.5 µm cells) (**Figure 4C**). However, on days 20 and 25, proportions of larger cells (37.5 µm) were five times lower in the metal-contaminated TAR C5-4F cultures than in metal-contaminated SG C10-3 cultures, suggesting a greater impact of metals on the SG C10-3 strain.

2. Effects of metal stress on the membrane proteomes of the A. pacificum strains

2.1. Effects of metal stress on the protein expression profiles

The protein expression profiles (PEPs) obtained for the SG C10-3 and the TAR C5-4F strains showed protein spots distributed in the range 22-131 kDa/3.8-6.8 pI and 23-123 kDa/4.0-6.0 pI, respectively (**Figures 5A and 5B, Figures 6A and 6B**).

Protein spot detection led to a total number of 82 ± 12 and 58 ± 12 spots on the membrane proteome of the SG C10-3 strain respectively grown in control and in metal-contaminated conditions. The total number of membrane proteins expressed by SG C10-3 in the metal cocktail was nearly significantly lower than in control conditions (Student's *t*-test: P= 0.0702, $0.05 < P^{*} \leq 0.10$) (**Figures 5A and 5B**).

For the TAR C5-4F strain, protein spot detection led to a total number of 101 ± 8 and 84 ± 5 spots on the membrane proteome of the TAR C5-4F strain respectively grown in control and in metal-contaminated conditions. The total number of membrane proteins expressed by TAR C5-4F in the metal cocktail was thus significantly lower than in control conditions (Student's *t*-test: P= 0.0325, $0.01 < P^{**} \leq 0.05$) (**Figures 6A and 6B**).

Finally, we found that the total number of spots on the membrane proteomes, obtained in metal-contaminated or in control conditions, was significantly higher for the TAR C5-4F strain than for the SG C10-3 strain (metal-contaminated conditions: P= 0.0229, $0.01 < P^{**} \leq 0.05$; control: P= 0.0921, $0.05 < P^{*} \leq 0.10$) (**Figures 5A and 5B, Figures 6A and 6B**).

2.2. Effects of metal stress on the membrane proteomes

LC-MS/MS identification and functional annotations for the membrane proteins expressed by the two *A. pacificum* strains are shown in **Tables 2** and **3**, respectively (**Supp Data 3 and 4**).

In comparison with controls, exposure to the multiple metals led to the following proportions of proteins of interest in the membrane proteomes of the two *A. pacificum* strains: 45%

proteins of interest for SG C10-3 and 38% for TAR C5-4F. Among these proteins principally down-regulated, (*i*) 34 disappeared from the membrane proteome of each *A. pacificum* strain, (*ii*) one was down-regulated (spot 1: -6.7) for SG C10-3 (**Figure 5C**), and two proteins were down-regulated for TAR C5-4F (spot 1: -11.5; spot 2: -16.7) (**Figure 6C**), (*iii*) whereas only one protein appeared for SG C10-3 (spot 23) (**Figure 5C**). Among the proteins disappearing from the SG C10-3 membrane proteome, five proteins were identified: actin (spot 3) and phospholipid scramblase (spot 5) (involved in cell transport), RUBISCO (spot 10) and CO_2 inducible periplasmic protein (spot 20) (key proteins involved in cell photosynthesis), and mitochondrial ATP synthase F1 beta subunit (spot 15) (involved in energy metabolism) (**Figure 5C**). Among the proteins disappearing from the TAR C5-4F membrane proteome, six proteins were identified: high-CO_2-inducible periplasmic protein (spots 22, 30 and 33) and light-harvesting protein (spots 26 and 35) (involved in photosynthesis), and ATP synthase CF1 beta chain (spot 34) (involved in energy metabolism) (**Figure 6C**).

Discussion

1. *Effects of metal stress on cell growth and morphometry of the Alexandrium pacificum strains*

The characterization of cell growth and morphometry under metal stress highlighted differences between the SG C10-3 and TAR C5-4F strains, suggesting intraspecific variability in response to contamination. Indeed, the SG C10-3 strain showed higher susceptibility in cell growth and morphometry to metals than the TAR C5-4F strain, for which no significant effect on these parameters was observed in the tested conditions. For SG C10-3, the metal cocktail induced increased cell sizes and delayed cell growth, but not for TAR C5-4F. Similarly, chromium stress inhibits cell growth in the green microalga *Micrasterias denticulate* (Volland

et al., 2014) and cadmium stress reduces growth in maize (Figlioli et al., 2019), and in rhizosphere bacteria (Kowalkowski et al., 2019).

Some studies mention that delays in cell division can lead to increased cell sizes (Vadia and Levin, 2015). Indeed, delays in cell division results from increased interdivision time during which the cell sizes can increase too. Though not verified in the present study, our results suggest that the delayed SG C10-3 growth also could result from increased interdivision time in response to metal stress, potentially contributing to the observed increase in SG C10-3 cell size.

Intraspecific variability observed in the cell growth and morphometry can also be explained by various genomic/proteomic regulations of the strains exposed to metal stress. The TAR C5-4F strain has probably developed a best adaptive response leading to nearly normal growth when exposed to metal contamination, in comparison to the SG C10-3 strain which showed disturbed growth and morphometry in metal-contaminated conditions.

2. Effects of metal stress on the membrane proteomes expressed by the A. pacificum strains

2.1. Comparison of the membrane proteomes expressed by the *A. pacificum* strains

Analysis of the membrane proteomes revealed distinct/specific PEPs for the *A. pacificum* strains, regardless of the experimental conditions tested (metal-contaminated or control). A proteomic approach applied on two distinct *Trypanosoma cruzi* strains also revealed significant differences in their expression profiles (181 proteins were considered common, 119 were found solely in a first strain, and 114 proteins were present exclusively in the second strain) (Kikuchi et al., 2010). In our study, the membrane proteomes showed significant differences in their constitutive total number of proteins, which was significantly higher for TAR C5-4F than for SG C10-3, across both tested conditions (metal-contaminated or control).

Similarly, intraspecific variability of three strains of *Vibrio tapetis* depicted different numbers of protein spots in 2D-gels despite loading the same quantities of proteins (there were 729±13, 681±2 and 556±6 spots for the three respective strains, with similarity of 79% found between two of them, whereas the third showed similarities lower than 70%) (Balboa et al., 2011). For *A. pacificum*, this means that TAR C5-4F expresses a greater panel of membrane proteins, which may be used by the cells to better survive in the presence of metals, without be affected in its growth.

The membrane proteomes were made of proteins that differed between the two strains, with only three identified proteins expressed in common (ATP synthase, high-CO_2-inducible periplasmic protein, and light-harvesting protein). In both strains, part of the total membrane proteome remained unchanged in expression under metal stress (55% of the membrane proteome is unchanged for SG C10-3, and 62% for TAR C5-4F). In SG C10-3, the unchanged proteins were identified as HSP 90 known for its chaperone activity (Jean et al., 2017), peridinin chlorophyll *a* binding protein involved in photosynthesis (Jean et al., 2017), and mitochondrial ATP synthase F1 beta subunit (**Figure 5C**), whereas in TAR C5-4F, these unchanged proteins were ferredoxin-NADP(+) reductase involved in the photophosphorylation step of photosynthesis (Jean et al., 2017), chloroplast cytochrome *f* known for its role in respiratory and photosynthetic electron transport (Hurt and Hauska, 1981) and ATP synthase CF1 beta chain involved in energy metabolism (Jean et al., 2017) (**Figure 6C**). As a result, involved in photosynthesis, chaperone activity or energy metabolism, these unchanged proteins can be candidates for maintaining each strain in its respective metal-contaminated ecosystem.

2.2. Effects of metal stress on the *A. pacificum* membrane proteomes

Under metal stress, the proteins of interest were principally down-regulated, with total numbers of spots constituting the membrane proteomes significantly lower than in controls, for both studied *A. pacificum* strains. The proteins of interest (changing in expression in response to metal stress) represented 45% of the membrane proteome expressed by SG C10-3, compared with 38% of the membrane proteome expressed by TAR C5-4F. The higher susceptibility in terms of growth of the SG C10-3 strain exposed to metal stress, relatively to TAR C5-4F, may result from its higher percentage of down-regulated membrane proteins in these metal-contaminated conditions. It exists a strong relationship between the cell cycle and the protein expression, as shown in investigations about changes in the proteome during the cell cycle of *Prorocentrum triestinum* (Chan et al. 2004). Significant fluctuations in the relative abundance of proteins were observed during the cell cycle of this dinoflagellate: preblooming proteins PB1, PB2, and PB3 were prominently found in the vegetative stages but blooming-related proteins BP1 and BP2 were expressed at high abundance and greatly enhanced in the blooming stages. Indeed, the growth cycle controls the DNA cycle which is mediated through the attainment of a level of protein necessary for DNA replication (Alberghina and Sturani, 1981). In our study, the higher down-regulation (or degradation) of some proteins, subsequent to metal exposure, could further impact the growth of SG C10-3 strain, relatively to TAR C5-4F.

As detailed below, several biological functions in the cells of the studied strains may be affected by the changes in their protein expression under polymetallic contamination. These disturbed functions include cell transport (changes in expression of actin and phospholipid scramblase), photosynthesis (changes in expression of high-CO_2-inducing periplasmic protein, RUBISCO, and light-harvesting protein), and energy metabolism (changes in expression of ATP synthase).

2.2.1. Effects of metal contamination on cell transport proteins

Cytoskeletal actin disappeared specifically from the proteome of the *A. pacificum* SG C10-3 strain. Similarly, in the alga *Spirogyra decimina*, actin gradually disappeared with increasing time and cadmium concentration, which indicated disruption of the actin cytoskeleton (Pribyl et al., 2005).

Actin is a family of multi-functional proteins that form microfilaments in the cytoskeleton of all eukaryotic cells (Hall, 1998). Mg^{2+} and Ca^{2+} are involved in the polymerization of actin (Maruyama et al., 1981) and some metals may act similarly to Ca^{2+} (cadmium and calcium have similar ionic radii). Actin participates in many important cellular processes, including cell motility, vesicle and organelle movement, cell signaling, establishment and maintenance of cell junctions/shape, cytokinesis, and cell division (Soyer-Gobillard et al., 1996). As a result, in the present study, the down-regulation (or degradation) of actin in SG C10-3 may help explain the delay in cell growth and the subsequent increase in cell size observed in metal-contaminated conditions (not occurring in the TAR C5-4F strain).

The phospholipid scramblase, down-regulated in the SG C10-3 cells exposed to metal stress, belongs to a family of transmembrane proteins responsible for the Ca^{2+} mediated-bidirectional phospholipid translocation in plasma membranes (Sivagnanam et al., 2017). Divalent metals may mimic calcium (Fox et al., 1998), especially during scramblase-mediated Ca^{2+} transport into the cells. Consequently, the down-regulation of scramblase in SG C10-3 may reduce metal toxicity in cells by limiting metal entry through the plasma membrane, which may help this strain adapt and/or be resistant to metal stress. Many reports have shown the multifunctional roles of phospholipid scramblase in key cellular processes, including protein/DNA interactions, transcriptional regulation and apoptosis. Trace metals such as cadmium, chromium, lead, and mercury are known to induce apoptosis, *via* proteins like phospholipid scramblase (Pulido and Parrish, 2003). In our study, down-regulation of

phospholipid scramblase in SG C10-3 cells may lead to less apoptosis at the end of its growth, as observed for this strain during the stationary phase.

2.2.2. Effects of metal contamination on photosynthetic proteins

Decreases in the abundance of many photosynthetic proteins (high-CO_2-inducing periplasmic protein, RUBISCO, and light-harvesting protein) were recorded, indicating that photosynthesis is a metabolic pathway sensitive to metal contamination in *A. pacificum* cells. This echoes many studies reporting the harmful effects of metals on photosynthesis, either by chlorophyll degradation, or by destruction of chloroplast ultrastructure and down-regulation of many proteins involved in the Calvin cycle (Gillet et al., 2006; Führs et al., 2008; Kieffer et al., 2008; Ahsan et al., 2009).

Regarding the high-CO_2-inducing periplasmic protein, this protein disappeared from the membrane proteomes of both studied strains in contaminated conditions. Among the molecular mechanisms developed by photosynthetic organisms to acclimate and adapt in response to high CO_2 concentrations needed by photosynthesis, expression of multiple high-CO_2-inducible periplasmic proteins has been shown, for example in the extracellular proteome of the unicellular green alga *Chlamydomonas reinhardtii* exposed to 3% CO_2 in air for three days (Hanawa et al., 2007; Baba et al., 2011). The high-CO_2-inducible periplasmic H43/Fea1 homologous genes are expressed by the chlorophytes *Scenedesmus obliquus*, *Chlorococcum littorale*, *Volvox carteri*, and the dinoflagellate *Heterocapsa triquetra* (Allen et al., 2007). This protein, involved in the iron-assimilation pathway, is linked to changes in CO_2 concentration (Sasaki et al., 1998; Allen et al., 2007). For example, H43/Fea1 is the most abundant extracellular soluble protein (26%) expressed by the high-CO_2 (3%)-grown cells of *C. reinhardtii* (Baba et al., 2011). A homology search of DNA sequences showed that H43/Fea1 expression is induced in *C. reinhardtii* cells by iron deficiency (< 1 μM) and by

excessive levels of cadmium (> 25 μM), which show contrasted responses of this green alga in response to metal exposure (Rubinelli et al., 2002; Allen et al., 2007).

Thanks to RUBISCO, photosynthetic microorganisms use CO_2 efficiently during the Calvin cycle of photosynthesis. However, RUBISCO, which catalyzes carboxylation of the substrate ribulose-1,5-bisphosphate (RuBP) during the second step of photosynthesis (Reumann and Weber, 2006), disappeared in the membrane proteome of the metal-contaminated SG C10-3 cultures. Some studies have also shown that trace metals decrease RUBISCO abundance in *A. pacificum* ACT03, *Zea mays*, and the microalga *Pseudokirchneriella subcapitata* (Vannini et al., 2009; Jean et al., 2017; Figlioli et al., 2019). The known high RUBISCO sensitivity to metal-induced oxidative conditions, which leads to methionine sulfoxide residues then targeted for ubiquitination, may increase its proteolytic degradation (Ge et al., 2009). Similarly, significant decreases in RUBISCO activity have been observed in the aquatic plant *Salvinia natans* contaminated by metals (Dhir et al., 2011). The main consequence of this decrease may be lower CO_2 assimilation by the cells (Dhir et al., 2011), and lower efficiency of RuBP recycling (which is a substrate of the Calvin cycle) (Kieffer et al., 2008).

In our study, a light-harvesting polyprotein precursor and a light-harvesting protein were under-expressed by the TAR C5-4F strain in metal-contaminated conditions. Light-harvesting complex of a photosystem (functional unit in photosynthesis) is made of subunit proteins and photosynthetic pigments. The constituent transmembrane proteins, occurring in the reaction center of photosystem II, bind to chlorophyll *a* and beta-carotene, and pass the excitation energy on to the reaction center (Barber, 2002; Standfuss et al., 2005). These light-harvesting protein complexes are used by photosynthetic organisms to collect more of the incoming light than would be captured by the photosynthetic reaction center alone. In the alga *Euglena gracilis*, the polyprotein precursor of the light-harvesting chlorophyll *a/b* binding protein of photosystem II (LHCPII) is inhibited in the presence of Zn^{2+} and Cu^{2+} (Enomoto et al., 1997).

Similarly, in the diatom *Thalassiosira pseudonana*, the transcription of three *LI818*–like genes (*Lhcx1*, *Lhcx5*, *and Lhcx6*) is down-regulated under iron or copper deprivation, whereas the protein encoded by *Lhcx1* is up-regulated under iron limitation (Zhu et al., 2010).

2.2.3. Effects of metal contamination on energy metabolism proteins

In response to the tested metal stress conditions, ATP synthase F1 beta subunit and the membrane mitochondrial ATP synthase CF1 beta chain disappeared from the membrane proteomes of the SG C10-3 and TAR C5-4F strains, respectively. These subunits belong to a large ATP-synthase complex located in the mitochondrial membranes, which converts ADP and orthophosphate during oxidative phosphorylation of cell respiration, into ATP-energy rich molecules (Kühlbrandt, 2015). Few studies report similar results, except regarding the effects of trace metals on the ATP-synthase activity that decreased in the plasma membrane fraction of wheat and sunflower roots that had been exposed to cadmium treatments (Fodor et al., 1995). Consequently, reduced ATP-synthase activity and subsequent ATP synthesis may correspond to a decreased aerobic pathway/mitochondrial respiratory chain, leading to less O_2 consumption and less associated reactive oxygen species (ROS) production, which may counteract the quantities of ROS generated by the metal stress, and thus, helping limit the oxidative stress.

Conclusion

This study explored modifications in the membrane proteomes, cell growth, and morphometry in two distinct Mediterranean strains of *A. pacificum*, in response to exposure to a metal cocktail. Cell growth and morphometry were different between strains in these conditions. Susceptibility of SG C10-3 to metals was high during its growth, with an increase in cell size, which was not observed for TAR C5-4F. This intraspecific variability may be related to

different biomolecular regulations in these strains coming from metal-contaminated ecosystems. The total number of proteins constituting the membrane proteome of TAR C5-4F was higher than that of SG C10-3, which may help this strain to better adapt and/or be resistant to metal-contaminated conditions. However, metal stress led to mainly down-regulated proteins of interest, showing the harmful effects of metals on the membrane proteomes from both strains. These proteomic modifications may affect metabolic functions in SG C10-3 and TAR C5-4F cells, such as cell transport, photosynthesis, and energy metabolism. However, other modifications observed in their membrane proteomes may promote adaptation and/or resistance to metal stress, contributing, more generally, to an increase in the occurrence, distribution, and intensity of the *A. pacificum* HAB, particularly in marine metal-contaminated ecosystems.

Acknowledgements

This work was supported by the research network GdR "PHYCOTOX: Des micro-algues aux risques pour l'Homme et l'écosystème". We would like to thank D[rs] Antonella Luglié and Esther Garcés for providing us the *A. pacificum* strains used in this study, and D[rs] Yong Zhang and Da-Zhi Wang (State Key Laboratory of Marine Environmental Science/College of the Environment and Ecology, Xiamen University, Xiamen, P.R. China) for the *A. pacificum* protein database sequences used for protein identification.

References

Ahsan, N., Renaut, J., and Komatsu, S. (2009). Recent developments in the application of proteomics to the analysis of plant responses to heavy metals. Proteomics 9, 2602–2621.

Alberghina, L., and Sturani, E. (1981). Control of growth and of the nuclear division cycle in *Neurospora crassa*. Microbiol. Rev. 45, 99-122.

Allen, M.D., Del Campo, J.A., Kropat, J., and Merchant, S.S. (2007). FEA1, FEA2, and FRE1, encoding two homologous secreted proteins and a candidate ferrireductase, are expressed coordinately with FOX1 and FTR1 in iron-deficient *Chlamydomonas reinhardtii*. Eukaryot. Cell 6, 1841–1852.

Aloui, A., Recorbet, G., Lemaître-Guiller, C., Mounier, A., Balliau, T., Zivy, M., Wipf, D., Dumas-Gaudot, E. (2018). The plasma membrane proteome of *Medicago truncatula* roots as modified by arbuscular mycorrhizal symbiosis. Mycorrhiza 1, 1-16.

Anderson, D.M., Alpermann, T.J., Cembella, A.D., Collos, Y., Masseret, E., and Montresor, M. (2012). The globally distributed genus *Alexandrium*: multifaceted roles in marine ecosystems and impacts on human health. Harmful Algae 14, 10–35.

Baba, M., Suzuki, I., Shiraiwa, Y. (2011). Proteomic analysis of high-CO_2-inducible extracellular proteins in the unicellular green alga, *Chlamydomonas reinhardtii*. Plant Cell Physiol. 52, 1302–1314.

Bae, M.S., Cho, E.J., Choi, E.Y., Park, O.K. (2003). Analysis of the *Arabidopsis* nuclear proteome and its response to cold stress. Plant J. 36, 652-663.

Balboa, S., Bermudez-Crespo, J., Gianzo, C., López, J.L., and Romalde, J.L. (2011). Proteomics and multilocus sequence analysis confirm intraspecific variability of *Vibrio tapetis*. FEMS Microbiol. Lett. 324, 80–87.

Barber, J. (2002). Photosystem II: a multisubunit membrane protein that oxidises water. Curr. Opin. Struct. Biol. 12, 523–530.

Bordier, C. (1981). Phase separation of integral membrane proteins in Triton X-114 solution. J. Biol. Chem. 256, 1604–1607.

Bravo, I., Vila, M., Masó, M., Figueroa, R.I., and Ramilo, I. (2008). *Alexandrium catenella* and *Alexandrium minutum* blooms in the Mediterranean Sea: Toward the identification of ecological niches. Harmful Algae 7, 515–522.

Chan, L.L., Hodgkiss, I.J., Man-Fan Wan, J., Hon-Kei Lum, J., Sin-Chi Mak, A., Sit, W.-H. et al. (2004). Proteomic study of a model causative agent of harmful algal blooms, *Prorocentrum triestinum* II: The use of differentially expressed protein profiles under different growth phases and growth conditions for bloom prediction. Proteomics, 4, 3214-3226.

Chetouhi, C., Laabir, M., Masseret, E., and Jean, N. (2019). In silico prediction of the secretome from the invasive neurotoxic marine dinoflagellate *Alexandrium catenella*. Environ.

Dhir, B., Sharmila, P., Pardha Saradhi, P., Sharma, S., Kumar, R., and Mehta, D. (2011). Heavy metal induced physiological alterations in *Salvinia natans*. Ecotoxicol. Environ. Saf. 74, 1678–1684.

Enomoto, T., Sulli, C., Schwartzbach, S.D. (1997). A soluble chloroplast protease processes the Euglena [Mastigophora] polyprotein precursor to the light harvesting chlorophyll a/b binding protein of photosystem, 2. Plant Cell Physiol. 38, 743–746.

Fertouna-Bellakhal, M., Dhib, A., Fathalli, A., Bellakhal, M., Chomérat, N., Masseret, E., et al. (2015). *Alexandrium pacificum* Litaker sp. nov (Group IV): Resting cyst distribution and toxin profile of vegetative cells in Bizerte Lagoon (Tunisia, Southern Mediterranean Sea). Harmful Algae 48, 69–82.

Figlioli, F., Sorrentino, M.C., Memoli, V., Arena, C., Maisto, G., Giordano, S., et al. (2019). Overall plant responses to Cd and Pb metal stress in maize: Growth pattern, ultrastructure, and photosynthetic activity. Environ. Sci. Pollut. Res. Int. 26, 1781–1790.

Fodor, E., Szabó-Nagy, A., Erdei, L. (1995). The Effects of Cadmium on the Fluidity and H+-ATPase Activity of Plasma Membrane from Sunflower and Wheat Roots. J. Plant Physiol. 147, 87–92.

Fox, D.A., He, L., Poblenz, A.T., Medrano, C.J., Blocker, Y.S., Srivastava, D. (1998). Lead-induced alterations in retinal cGMP phosphodiesterase trigger calcium overload, mitochondrial dysfunction and rod photoreceptor apoptosis. Toxicol. Lett. 102–103, 359–361.

Führs, H., Hartwig, M., Molina, L.E.B., Heintz, D., Van Dorsselaer, A., Braun, H.-P., et al. (2008). Early manganese-toxicity response in *Vigna unguiculata* L.-a proteomic and transcriptomic study. Proteomics 8, 149–159.

Garnier, C., Mounier, S., and J.-Y. Benaïm (2004). Metal logarithmic scale titration as a tool for complexing ligand distribution determination: an application by DPASV. Environ Technol 25, 589–599.

Ge, C., Ding, Y., Wang, Z., Wan, D., Wang, Y., Shang, Q., et al. (2009). Responses of wheat seedlings to cadmium, mercury and trichlorobenzene stresses. J. Environ. Sci. 21, 806–813.

Gillet, S., Decottignies, P., Chardonnet, S., and Le Maréchal, P. (2006). Cadmium response and redoxin targets in *Chlamydomonas reinhardtii*: a proteomic approach. Photosynth. Res. 89, 201–211.

Guillard, R.R., and Ryther, J.H. (1962). Studies of marine planktonic diatoms. I. *Cyclotella nana* Hustedt, and *Detonula confervacea* (cleve) Gran. Can. J. Microbiol. 8, 229–239.

Hadjadji, I., Frehi, H., Ayada, L., Abadie, E., and Collos, Y. (2014). A comparative analysis of *Alexandrium catenella/tamarense* blooms in Annaba Bay (Algeria) and Thau Lagoon (France); phosphorus limitation as a trigger. C. R. Biol. 337, 117–122.

Hall, A. (1998). Rho GTPases and the actin cytoskeleton. Science 279, 509–514.

Hall, J. L. (2002). Cellular mechanisms for heavy metal detoxification and tolerance. J. Exp. Bot. 53, 366, 1–11.

Hallegraeff, G.M. (1993). A review of harmful algal blooms and their apparent global increase. Phycologia 32, 79–99.

Hanawa, Y., Watanabe, M., Karatsu, Y., Fukuzawa, H., and Shiraiwa, Y. (2007). Induction of a high-CO2-inducible, periplasmic protein, H43, and its application as a high-CO_2-responsive marker for study of the high-CO_2-sensing mechanism in *Chlamydomonas reinhardtii*. Plant Cell Physiol. 48, 299–309.

Herzi, F., Jean, N., Sakka Hlaili, A., and Mounier, S. (2014). Three-dimensional (3-D) fluorescence spectroscopy analysis of the fluorescent dissolved organic matter released by the marine toxic dinoflagellate *Alexandrium catenella* exposed to metal stress by zinc or lead. J. Phycol. 50, 665–674.

Herzi, F., Jean, N., Zhao, H., Mounier, S., Mabrouk, H.H., and Hlaili, A.S. (2013). Copper and cadmium effects on growth and extracellular exudation of the marine toxic dinoflagellate *Alexandrium catenella*: 3D-fluorescence spectroscopy approach. Chemosphere 93, 1230–1239.

Hoagland, P., Anderson, D.M., Kaoru, Y., and White, A.W. (2002). The economic effects of harmful algal blooms in the United States: Estimates, assessment issues, and information needs. Estuaries 25, 819–837.

Hurt, E., and Hauska, G. (1981). A cytochrome f/b6 complex of five polypeptides with plastoquinol-plastocyanin-oxidoreductase activity from spinach chloroplasts. Eur. J. Biochem. 111, 591–595.

Jauzein, C., Collos, Y., Garcés, E., Vila, M., and Maso, M. (2008). Short-term temporal variability of ammonium and urea uptake by *Alexandrium catenella* (Dinophyta) in cultures. J. Phycol. 44, 1136–1145.

Jean, N., Bogé, G., Jamet, J.-L., Richard, S., and Jamet, D. (2005). Annual contribution of different plankton size classes to particulate dimethylsulfoniopropionate in a marine perturbed ecosystem. J. Mar. Syst. 53, 235–247.

Jean, N., Dumont, E., Durrieu, G., Balliau, T., Jamet, J.-L., Personnic, S., et al. (2012). Protein expression from zooplankton communities in a metal contaminated NW mediterranean coastal ecosystem. Mar. Environ. Res. 80, 12–26.

Jean, N., Dumont, E., Herzi, F., Balliau, T., Laabir, M., Masseret, E., et al. (2017). Modifications of the soluble proteome of a mediterranean strain of the invasive neurotoxic dinoflagellate *Alexandrium catenella* under metal stress conditions. Aquat. Toxicol. 188, 80–91.

John, U., Litaker, R.W., Montresor, M., Murray, S., Brosnahan, M.L., and Anderson, D.M. (2014). Formal revision of the *Alexandrium tamarense* species complex (Dinophyceae) taxonomy: The introduction of five species with emphasis on molecular-based (rDNA) classification. Protist 165, 779–804.

Kieffer, P., Dommes, J., Hoffmann, L., Hausman, J.-F., and Renaut, J. (2008). Quantitative changes in protein expression of cadmium-exposed poplar plants. Proteomics 8, 2514–2530.

Kikuchi, S.A., Sodré, C.L., Kalume, D.E., Elias, C.G.R., Santos, A.L.S., de Nazaré Soeiro, M., Meuser, M., et al. (2010). Proteomic analysis of two *Trypanosoma cruzi zymodeme* 3 strains. Exp. Parasitol. 126, 540–551.

Kowalkowski, T., Krakowska, A., Złoch, M., Hrynkiewicz, K., and Buszewski, B. (2019). Cadmium-affected synthesis of exopolysaccharides (EPS) by rhizosphere bacteria. J. Appl. Microbiol. 127, 713–723.

Kühlbrandt, W. (2015). Structure and function of mitochondrial membrane protein complexes. BMC Biol. 13, 89.

Laabir, M., Collos, Y., Masseret, E., Grzebyk, D., Abadie, E., Savart, V., Sibat, M., et al. (2013). Influence of environmental factors on the paralytic shellfish toxin content and profile of *Alexandrium pacificum* (Dinophyceae) isolated from the Mediterranean Sea. Mar. Drugs 11, 1583–1601.

Laabir, M., Jauzein, C., Genovesi, B., Masseret, E., Grzebyk, Cecchi, P., et al. (2011). Influence of temperature, salinity and irradiance on the growth and cell yield of the harmful red tide dinoflagellate *Alexandrium catenella* colonizing Mediterranean waters. J. Plankton Res. 33, 1550-1563.

Laemmli, K. (1970). Cleavage of structural proteins during the assembly of the bacteriophage T4. Nature 227, 680-685.

Langella, O., Valot, B., Balliau, T., Blein-Nicolas, M., and Bonhomme, L. (2017). X!TandemPipeline: a tool to manage sequence redundancy for protein inference and phosphosite identification. J. Proteome Res. 2, 494–503.

Linares, D., Jean, N., Van Overtvelt, P., Ouidir, T., Hardouin, J., Blache, Y., et al. (2016). The marine bacteria *Shewanella frigidimarina* NCIMB400 up regulates the type VI secretion system during early biofilm formation. Environ. Microbiol. Rep. 8, 110–121.

Lowry, O.H., Rosebrough, N.J., Farr, A.L., and Randall, R.J. (1951). Protein measurement with the Folin phenol reagent. J. Biol. Chem. 193, 265–275.

Luglié, A., Sechi, N., Oggiano, G., Sanna, G., and Tapparo, A. (2002). Ecological assessment of Santa Giusta Lagoon (Sardinia, Italy). Ann. Chim. 92, 239–247.

Maruyama, K., Mimura, N., Asano, A. (1981). Rheological studies on calcium-sensitive gelation of actin filaments by actinogelin. J. Biochem. 89, 317–319.

Masseret, E., Grzebyk, D., Nagai, S., Genovesi, B., Lasserre, B., Laabir, M., et al. (2009). Unexpected genetic diversity among and within populations of the toxic dinoflagellate *Alexandrium pacificum* as revealed by nuclear microsatellite markers. Appl. Environ. Microbiol. 75, 2037–2045.

Park, T.G., Lim, W.A., Park, Y.T., Lee, C.K., and Jeong, H.J. (2013). Economic impact, management and mitigation of red tides in Korea. Harmful Algae, Red Tides in Korea 30, S131–S143.

Penna, A., Garcès, E., Vila, M., Giacobbe, M.G., Fraga, S., Lugliè, A., et al. (2005). *Alexandrium catenella* (Dinophyceae), a toxic ribotype expanding in the NW Mediterranean Sea. Mar. Biol. 148, 13–23.

Pinedo, S., Jordana, E., Flagella, M.M., and Ballesteros, E. (2014). Relationships Between Heavy Metals Contamination in Shallow Marine Sediments with Industrial and Urban Development in Catalonia (Northwestern Mediterranean Sea). Water Air. Soil Pollut. 225, 2084–3000.

Pribyl, P., Cepák, V., Zachleder, V. (2005). Cytoskeletal alterations in interphase cells of the green alga *Spirogyra decimina* in response to heavy metals exposure: I. The effect of cadmium. Protoplasma 226, 231–240.

Pulido, M.D., Parrish, A.R. (2003). Metal-induced apoptosis: mechanisms. Mutat. Res. 533, 227–241.

Quod, J.P., Turquet, J. (1996). Ciguatera in Réunion Island (SW Indian Ocean): epidemiology and clinical patterns. Toxicon 34, 779–785.

Reumann, S., Weber, A.P.M. (2006). Plant peroxisomes respire in the light: some gaps of the photorespiratory C2 cycle have become filled-others remain. Biochim. Biophys. Acta 1763, 1496–1510.

Rubinelli, P., Siripornadulsil, S., Gao-Rubinelli, F., Sayre, R.T. (2002). Cadmium- and iron-stress-inducible gene expression in the green alga *Chlamydomonas reinhardtii*: evidence for H43 protein function in iron assimilation. Planta 215, 1–13.

Santoni, V., Molloy, M., Rabilloud, T. (2000). Membrane proteins and proteomics: Un amour impossible ? Electrophoresis 21, 1054–1070.

Sasaki, T., Kurano, N., Miyachi, S. (1998). Cloning and characterization of high-CO_2-specific cDNAs from a marine microalga, *Chlorococcum littorale*, and effect of CO_2 concentration and iron deficiency on the gene expression. Plant Cell Physiol. 39, 131–138.

Sivagnanam, U., Palanirajan, S.K., Gummadi, S.N. (2017). The role of human phospholipid scramblases in apoptosis: An overview. Biochim. Biophys. Acta Mol. Cell Res. 1864, 2261–2271.

Soyer-Gobillard, M.-O., Ausseil, J., Géraud, M.-L. (1996). Nuclear and cytoplasmic actin in dinoflagellates. Bio. Cell 87, 17–35.

Standfuss, J., Terwisscha van Scheltinga, A.C., Lamborghini, M., and Kühlbrandt, W. (2005). Mechanisms of photoprotection and nonphotochemical quenching in pea light-harvesting complex at 2.5 A resolution. EMBO J. 24, 919–928.

Tessier, E., Garnier, C., Mullot, J.-U., Lenoble, V., Arnaud, M., Raynaud, M., et al. (2011). Study of the spatial and historical distribution of sediment inorganic contamination in the Toulon bay (France). Mar. Pollut. Bull. 62, 2075–2086.

Uribe, P., Espejo, R.T. (2003). Effect of associated bacteria on the growth and toxicity of *Alexandrium pacificum*. Appl. Environ. Microbiol. 69, 659–662.

Vadia, S., Levin, P.A. (2015). Growth rate and cell size: A re-examination of the growth law. Curr. Opin. Microbiol. 24, 96–103.

Vannini, C., Marsoni, M., Domingo, G., Antognoni, F., Biondi, S., and Bracale, M. (2009). Proteomic analysis of chromate-induced modifications in *Pseudokirchneriella subcapitata*. Chemosphere 76, 1372–1379.

Vila, M., Garcés, E., Masó, and M., Camp, J. (2001). Is the distribution of the toxic dinoflagellate *Alexandrium catenella* expanding along the NW Mediterranean coast ? Mar. Ecol. Prog. Ser. 222, 73–83.

Volland, S., Bayer, E., Baumgartner, V., Andosch, A., Lütz, C., Sima, E., et al. (2014). Rescue of heavy metal effects on cell physiology of the algal model system *Micrasterias* by divalent ions. J. Plant Physiol. 171, 154–163.

Wang, D.-Z., Gao, Y., Lin, L., Hong, H.-S. (2013). Comparative proteomic analysis reveals proteins putatively involved in toxin biosynthesis in the marine dinoflagellate *Alexandrium catenella*. Mar. Drugs 11, 213–232.

Wang, D.-Z., Lin, L., Gu, H.-F., Chan, L.L., and Hong, H.-S. (2008). Comparative studies on morphology, ITS sequence and protein profile of *Alexandrium tamarense* and *A. pacificum* isolated from the China Sea. Harmful Algae 7, 106–113.

Wang, D.-Z., Zhang, S.-G., Gu, H.-F., Chan, L.L., and Hong, H.-S. (2006). Paralytic shellfish toxin profiles and toxin variability of the genus *Alexandrium* (Dinophyceae) isolated from the Southeast China Sea. Toxicon 48, 138–151.

Yoo, J.S., Shin, H.W. (2004). Effects of basic oxygen furnace slag and inorganic nutrients on the germination of resting cysts of two toxic dinoflagellates. J. Environ. Biol. 25, 147–150.

Zhang, Y., Zhang, S.-F., Lin, L., and Wang, D.-Z. (2014) Comparative transcriptome analysis of a toxin-producing dinoflagellate *Alexandrium catenella* and its non-toxic mutant. Mar. Drugs 12, 5698–5718.

Zhang, S.-F., Zhang, Y., Xie, Z.-X., Zhang, H., Lin, L., and Wang, D.-Z. (2015). iTRAQ-based quantitative proteomic analysis of a toxigenic dinoflagellate *Alexandrium catenella* and its non-toxic mutant. Proteomics 15, 4041–4050.

Zhang, Y., Zhang, S.-F., Lin, L., Wang, D.-Z. (2017). Whole Transcriptomic Analysis Provides Insights into Molecular Mechanisms for Toxin Biosynthesis in a Toxic Dinoflagellate *Alexandrium catenella* (ACHK-T). Toxins 9, 213.

Zhu, S.-H., Guo, J., Maldonado, M.T., and Green, B.R. (2010). Effects of Iron and Copper Deficiency on the Expression of Members of the Light-Harvesting Family in the Diatom *Thalassiosira pseudonana* (Bacillariophyceae). J. Phycol. 46, 974–981.

Declaration of interests

☒ The authors declare that they have no known competing financial interests or personal relationships that could have appeared to influence the work reported in this paper.

☐The authors declare the following financial interests/personal relationships which may be considered as potential competing interests:

Figure 1: Location of the sampling stations. (A) Sampling station for the *Alexandrium pacificum* SG C10-3 strain **(B)** Sampling station for the *A. pacificum* TAR C5-4F strain.

Figure 2: Schematic representation of the experimental procedure. (A) Cells were grown with or without metals for 30 days **(B)** Cells were counted, and their sizes measured, every 5 days during growth **(C)** After extraction, membrane proteins were separated by 2-D electrophoresis. Proteins (spots) of interest were picked to be identified by LC-MS/MS. Protein names/functions were determined with Uniprot/NCBI database queries.

Figure 3: Temporal change in cell densities (cells L^{-1}) during growth of *Alexandrium pacificum* **SG C10-3 and TAR C5-4F strains, in metal-contaminated and control conditions.**

Figure 4: Effects of metal stress on the cell size of the *Alexandrium pacificum* strains (A) Panel of the cell sizes measured between 22.5 µm (min) and 37.5 µm (max) **(B)** Boxplots of the temporal change in cell size distribution around the median: cell sizes for the SG C10-3 strain and the TAR C5-4F strain (C: control; CK: cocktail) **(C)** Temporal change in the proportions of cells in the different measured cell sizes (C: control; CK: cocktail).

Figure 5: Representative 2-D maps comparing the membrane proteomes of *Alexandrium pacificum* SG C10-3 obtained in control and metal-contaminated conditions. (**A**) Protein expression profile of the *Alexandrium pacificum* SG C10-3 strain grown under control conditions (**B**) Protein expression profile of the *Alexandrium pacificum* SG C10-3 strain grown in the metal cocktail. Proteins are identified by their spot numbers (**C**) Names of the proteins are shown with their fold differences in expression; in black (A): appeared proteins; in grey: down-regulated or (D) disappeared proteins; in white (-): proteins unchanged in expression. *: protein whose expression was nearly significantly different under metal-contaminated conditions ($0.05 < P^{*} \leq 0.10$).

Figure 6: Representative 2-D maps comparing the membrane proteomes of *Alexandrium pacificum* TAR C5-4F obtained in control and metal-contaminated conditions. (**A**) Protein expression profile of the *Alexandrium pacificum* TAR C5-4F strain grown under control conditions (**B**) Protein expression profile of the *Alexandrium pacificum* TAR C5-4F strain grown in metal-contaminated conditions. Proteins are identified by their spot numbers

(**C**) Names of the proteins are shown with their fold differences in expression; in grey: down-regulated or (D) disappeared proteins; in white (-): proteins unchanged in expression. *: protein whose expression was nearly significantly different under metal-contaminated conditions ($0.05 < P^{*} \leq 0.10$).

Table 1. *P* values (Student's test) for the comparison of cell densities and cell sizes during growth of the *Alexandrium pacificum* SG C10-3 and TAR C5-4F strains, in control and in metal-contaminated conditions

Days of growth	*Alexandrium pacificum SG C10-3* (Control *vs* Cocktail)		*Alexandrium pacificum TAR C5-4F* (Control *vs* Cocktail)	
	Cell density	Cell size	Cell density	Cell size
5	3.8E-02**	3.2E-05***	7.4E-01	4.8E-01
10	7.7E-02*	2.9E-02**	9.6E-01	5.8E-01
15	5.7E-02*	1.9E-07**	6.3E-01	8.9E-02*
20	8.0E-01	6.6E-02*	1.6E-01	8.9E-04***
25	4.9E-01	6.7E-02*	8.6E-01	5.8E-03***
30	4.4E-02**	3.2E-03***	1.4E-01	7.5E-01

*** highly significant: $P \leq 0.01$

** significant: $0.01 < P \leq 0.05$

* nearly significant: $0.05 < P \leq 0.10$

Table 2. Liquid chromatography-tandem mass spectrometry identification of the proteins constituting the membrane proteome of the *Alexandrium pacificum* SG C10-3 strain

Spot n°	Peptide number	MW (kDa) / pI		Protein name	Species Accession number	Putative function
		Obs	Theo			
3	2	41.7/3.9	41.7/5.3	Actin	*Alexandrium fundyense* ABO47874.1	Vesicular cellular import (20.09.18.09)
5	2	28.7/4.8	29.9/5.3	Phospholipid scramblase	*Perkinsus marinus* XP_002768242.1	Membrane lipid metabolism (01.06.02)
10	4	25.7/5.2	30.2/8.5	Ribulose-1,5-bisphosphate carboxylase	*Symbiodinium microadriaticum* OLP97657.1	Photosynthesis (02.30)
15	5	26.4/5.5	54.8/5.1	Mitochondrial ATP synthase F1 beta subunit	*Karlodinium veneficum* ADV91188.1	Transported compounds (20.01)
20	8	40.1/5.7	42.9/4.9	High-CO_2-inducible periplasmic protein	*Heterocapsa triquetra* AAW79380.1	Calcium binding (16.17.01)
24	6	29.3/5.1	81.6/5.0	HSP 90	*Karlodinium veneficum* ABI14419.1	Chaperone (14.01)
33	2	36.8/3.8	38.0/9.1	Peridinin-chlorophyll *a*-binding protein	*Symbiodinium* sp. AFH88375.1	Light absorption (02.45.03)
36	8	44.5/5.0	57.0/4.4	Hypothetical protein	*Aureococcus anophagefferens* XP_009037435.1	Unclassified protein (99)
37	15	47.1/5.2	57.0/4.4	Hypothetical protein	*Aureococcus anophagefferens* XP_009037435.1	Unclassified protein (99)
38	12	49.9/5.5	54.8/5.1	Mitochondrial ATP synthase F1 beta subunit	*Karlodinium veneficum* ADV91188.1	Transported compounds (20.01)
39	14	50.1/5.7	54.8/5.1	Mitochondrial ATP synthase F1 beta subunit	*Karlodinium veneficum* ADV91188.1	Transported compounds (20.01)
40	13	40.3/5.6	42.9/4.9	High-CO_2-inducible periplasmic protein	*Heterocapsa triquetra* AAW79380.1	Calcium binding (16.17.01)
41	3	44.8/5.7	30.2/8.5	Ribulose-1,5-bisphosphate carboxylase	*Symbiodinium microadriaticum* OLP97657.1	Photosynthesis (02.30)
48	2	99.5/5.4	30.2/8.5	Ribulose-1,5-bisphosphate carboxylase	*Symbiodinium microadriaticum* OLP97657.1	Photosynthesis (02.30)
49	2	108.2/5.1	45.9/8.3	Light-harvesting protein	*Symbiodinium* sp. CBI83418.1	Transmembrane signal transduction (30.05)

Table 3. Liquid chromatography-tandem mass spectrometry identification of the proteins constituting the membrane proteome of the *Alexandrium pacificum* TAR C5-4F strain

Spot n°	Peptide number	MW (kDa) / pI		Protein name	Species Accession number	Putative function
		Obs	Theo			
11	3	42.8/4.3	33.4/6.0	Unknown protein	-	-
22	9	41.5/4.3	42.9/4.9	High-CO_2-inducible periplasmic protein	*Heterocapsa triquetra* AAW79380.1	Calcium binding (16.17.01)
26	2	29.1/5.7	45.9/8.3	Light-harvesting protein	*Symbiodinium* sp. CBI83418.1	Transmembrane signal transduction (30.05)
30	9	41.7/5.2	42.9/4.9	High-CO_2-inducible periplasmic protein	*Heterocapsa triquetra* AAW79380.1	Calcium binding (16.17.01)
33	8	42.2/5.6	42.9/4.9	High-CO_2-inducible periplasmic protein	*Heterocapsa triquetra* AAW79380.1	Calcium binding (16.17.01)
34	6	24.5/5.8	53.2/5.1	ATP synthase CF1 beta chain	*Nageia nagi* YP_008965117.1	Transported compounds (20.01)
35	7	19.6/5.9	87.9/5.9	Light-harvesting polyprotein precursor	*Amphidinium carterae* CAA08771.1	Photosynthesis (02.30)
40	2	34.7/4.1	45.0/7.0	Chloroplast ferredoxin NADP(+) reductase	*Heterocapsa triquetra* AAW79380.1	Electron transport (20.01.15)
43	6	34.7/4.4	45.0/7.0	Chloroplast ferredoxin NADP(+) reductase	*Heterocapsa triquetra* AAW79380.1	Electron transport (20.01.15)
44	3	31.2/4.6	37.4/7.1	Chloroplast cytochrome *f*	*Heterocapsa triquetra* AAW79342.1	Electron transport (20.01.15)
47	2	45.4/4.4	53.2/5.1	ATP synthase CF1 beta chain	*Nageia nagi* YP_008965117.1	Transported compounds (20.01)

Highlights

- Growth inhibited under metal stress for *A. pacificum* SG C10-3, not for TAR C5-4F.
- SG C10-3 shows increased cell sizes under metal stress, not TAR C5-4F.
- Metals down-regulate proteins, decrease the number of proteins in the proteomes.
- Protein down-regulation affects photosynthesis/energy metabolism in both strains.
- Proteomic modifications promote cell adaptation in metal-contaminated ecosystems.

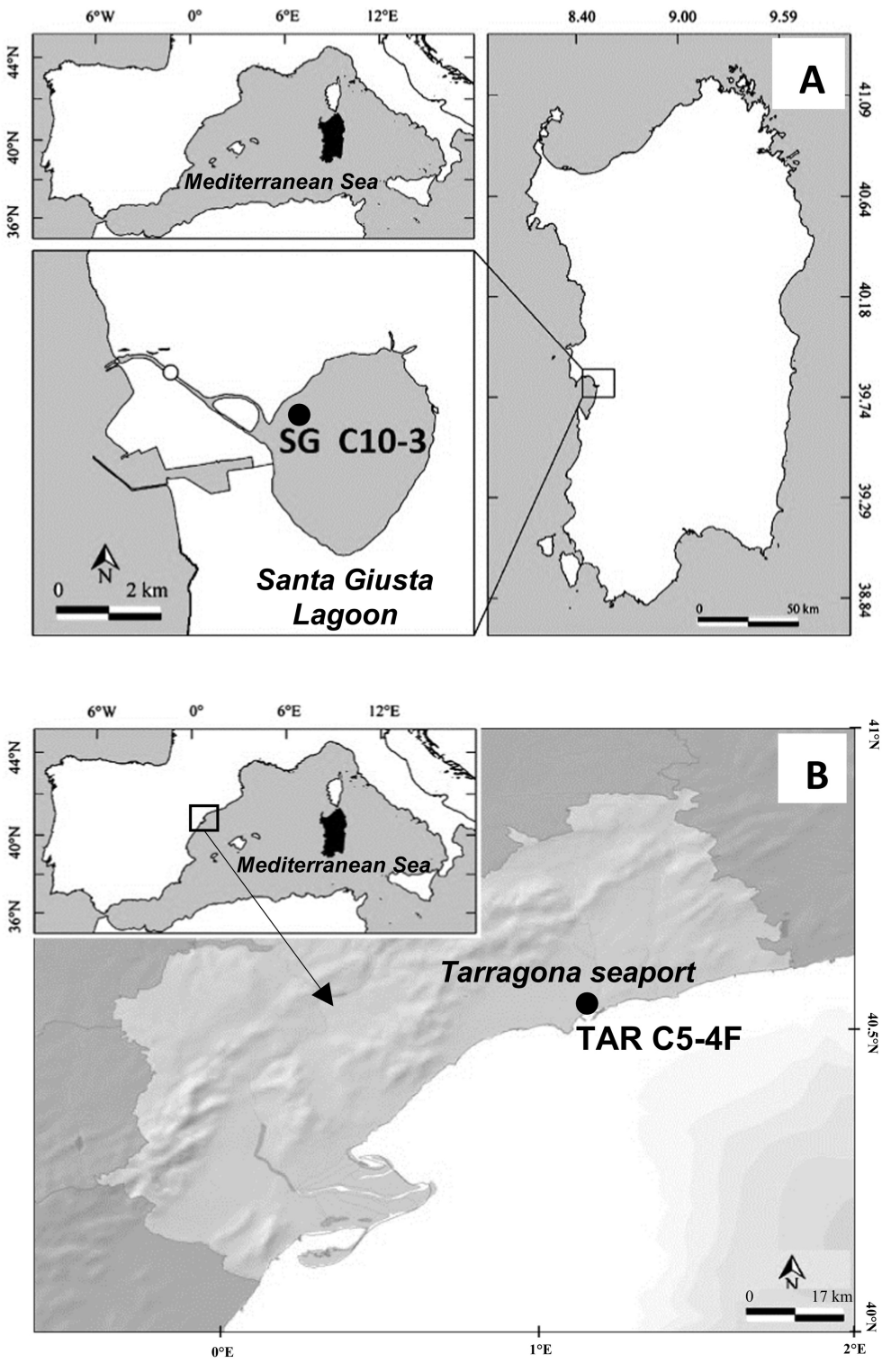
A
6°W
0°
6°E
12°E
44°N
40°N
36°N
Mediterranean Sea
8.40
9.00
9.59
41.09
40.64
40.18
39.74
39.29
38.84
SG C10-3
Santa Giusta
Lagoon
N
0
2 km
0
50 km
B
6°W
0°
6°E
12°E
44°N
40°N
36°N
Mediterranean Sea
41°N
40.5°N
40°N
Tarragona seaport
TAR C5-4F
N
0
17 km
0°E
1°E
2°E

Figure 1

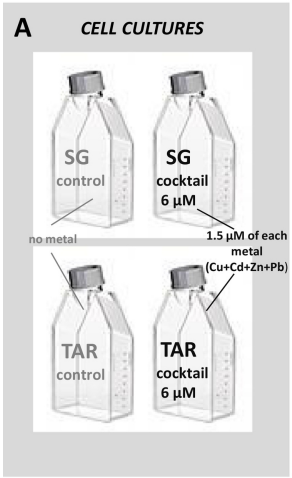
A
CELL CULTURES
SG
control
SG
cocktail
6 µM
no metal
1.5 µM of each
metal
(Cu+Cd+Zn+Pb)
TAR
control
TAR
cocktail
6 µM

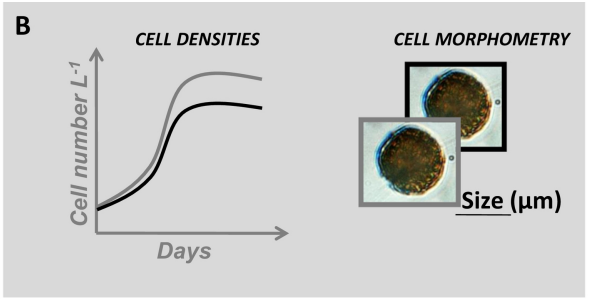
B
CELL DENSITIES
Cell number L-1
Days
CELL MORPHOMETRY
Size (µm)

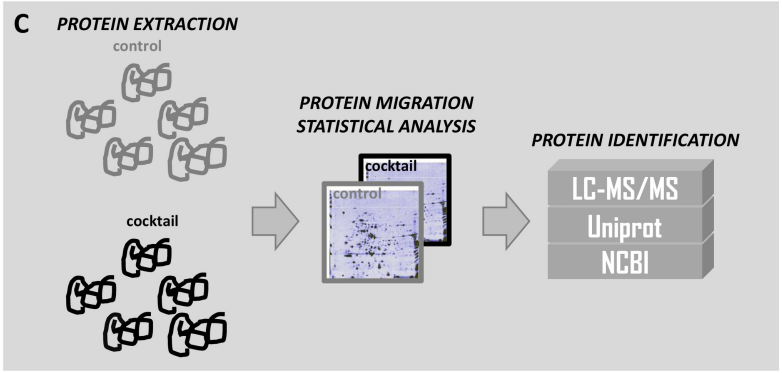
C
PROTEIN EXTRACTION
control
cocktail
PROTEIN MIGRATION
STATISTICAL ANALYSIS
cocktail
control
PROTEIN IDENTIFICATION
LC-MS/MS
Uniprot
NCBI

Figure 2

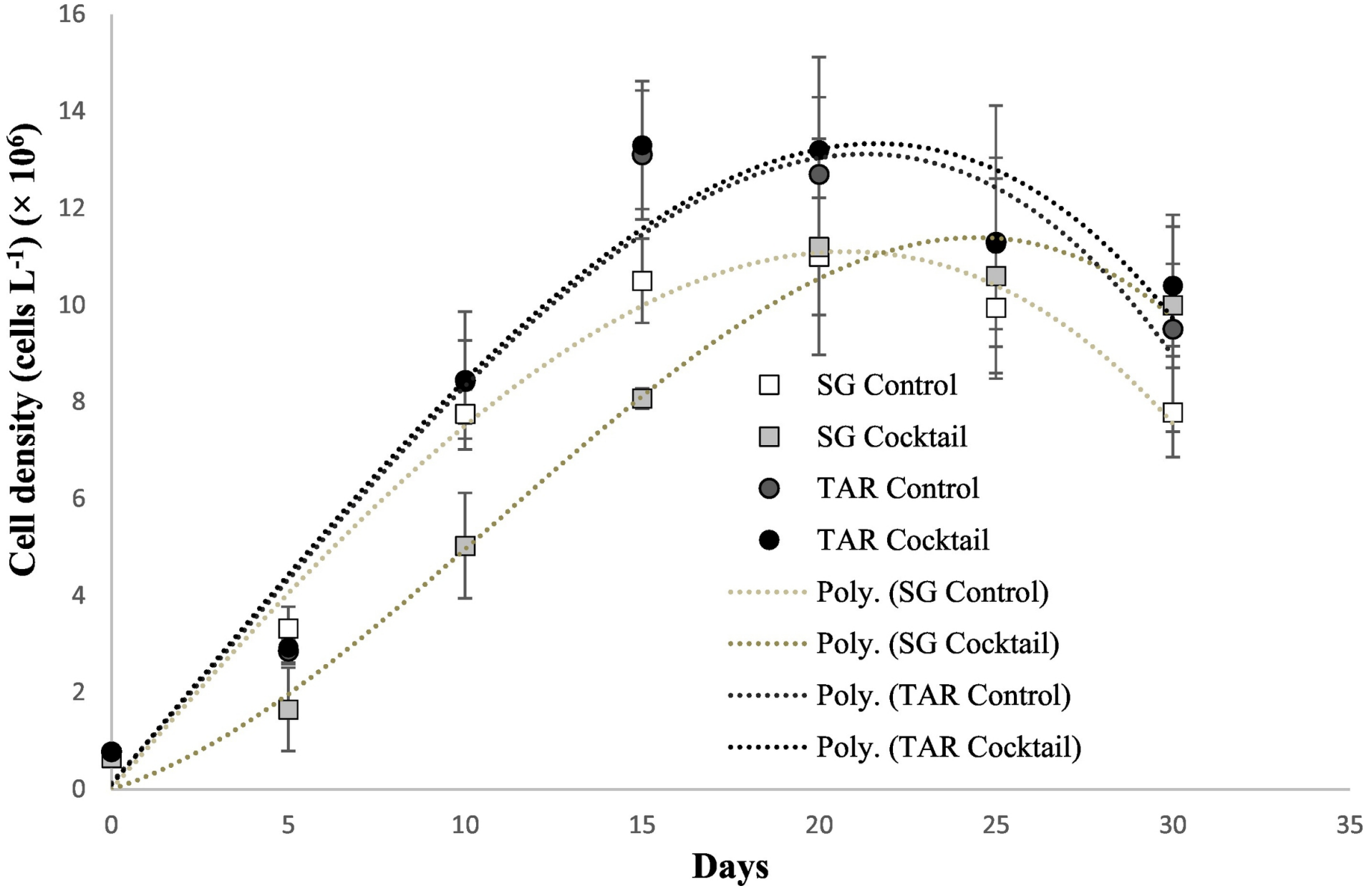
Cell density (cells L-1) (× 10⁶)
16
14
12
10
8
6
4
2
0
0
5
10
15
20
25
30
35
Days
SG Control
SG Cocktail
TAR Control
TAR Cocktail
Poly. (SG Control)
Poly. (SG Cocktail)
Poly. (TAR Control)
Poly. (TAR Cocktail)

Figure 3

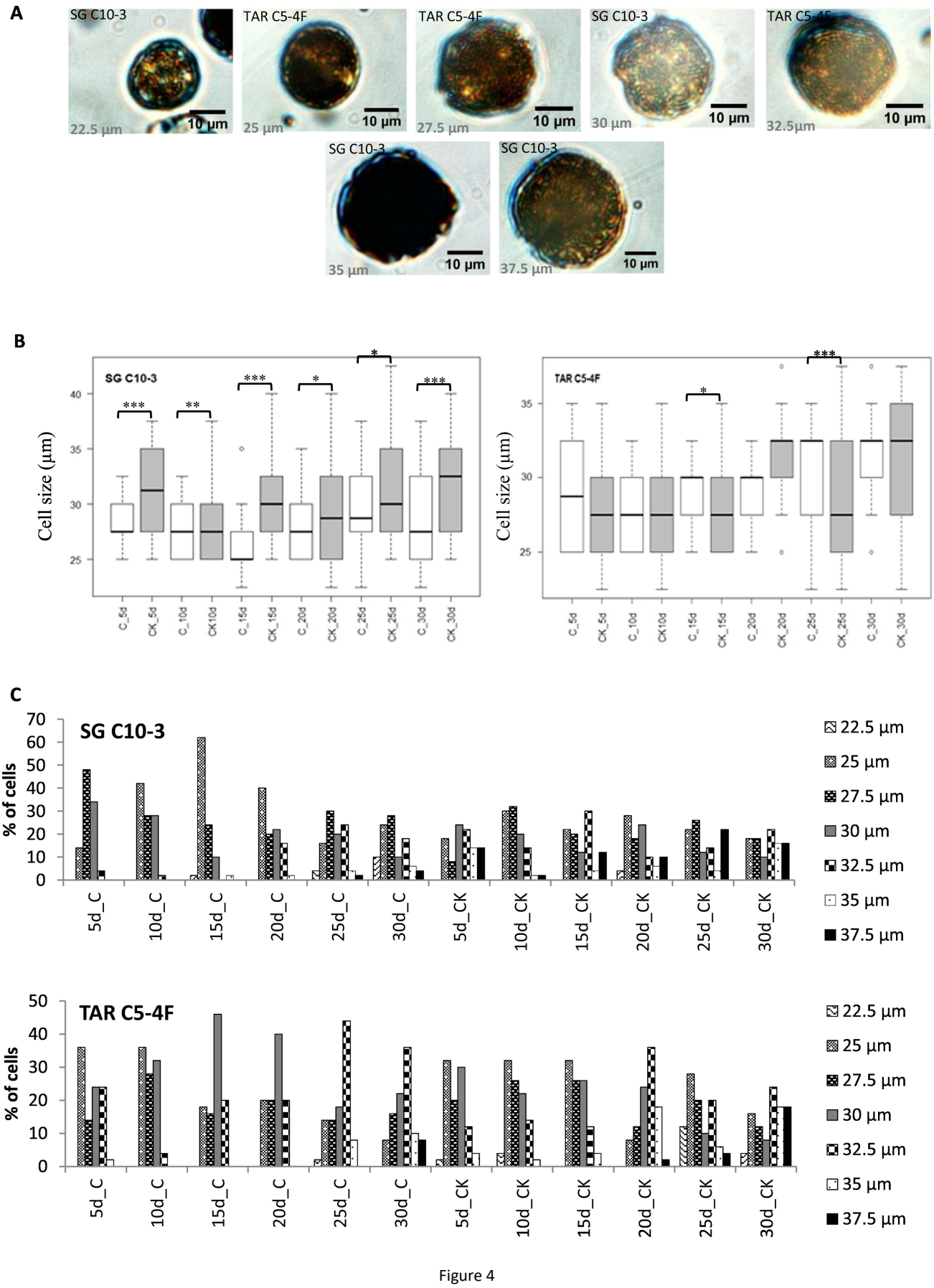
A
SG C10-3
22.5 μm
10 μm
TAR C5-4F
25 μm
10 μm
TAR C5-4F
27.5 μm
10 μm
SG C10-3
30 μm
10 μm
TAR C5-4F
32.5μm
10 μm
SG C10-3
35 μm
10 μm
SG C10-3
37.5 μm
10 μm
B
SG C10-3
Cell size (μm)
C_5d
CK_5d
C_10d
CK10d
C_15d
CK_15d
C_20d
CK_20d
C_25d
CK_25d
C_30d
CK_30d
TAR C5-4F
Cell size (μm)
C
SG C10-3
% of cells
5d_C
10d_C
15d_C
20d_C
25d_C
30d_C
5d_CK
10d_CK
15d_CK
20d_CK
25d_CK
30d_CK
22.5 μm
25 μm
27.5 μm
30 μm
32.5 μm
35 μm
37.5 μm
TAR C5-4F
% of cells

Figure 4

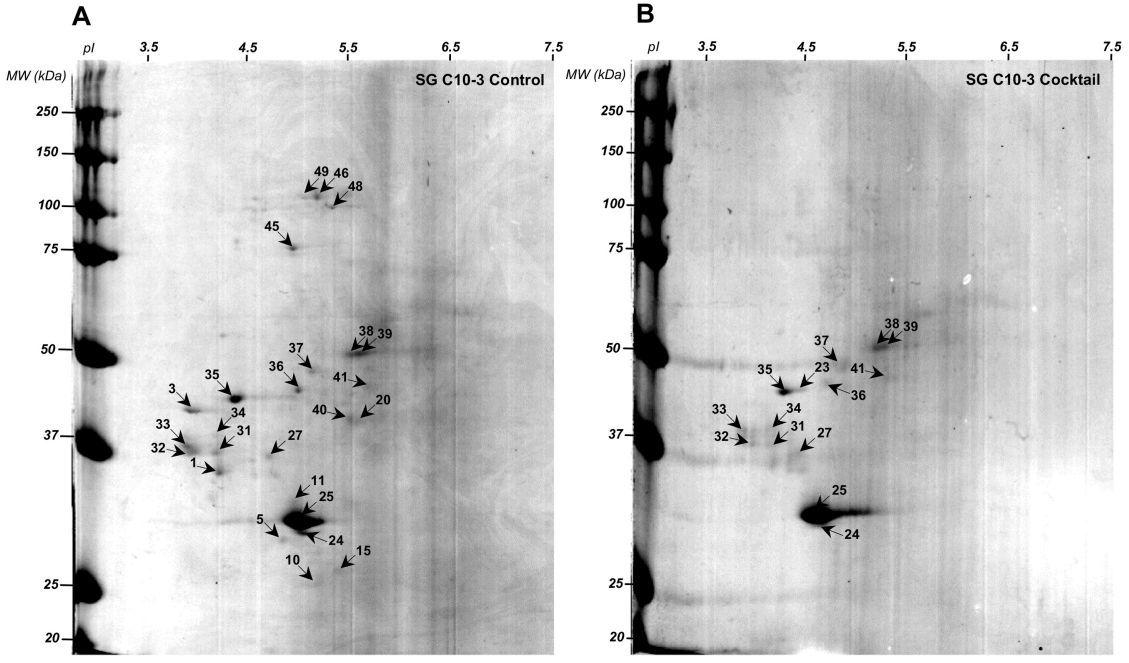

C

Spot n°	Protein name	Fold change
1	Unidentified protein	**-6.7***
3	Actin	**D**
5	Phospholipid scramblase	**D**
10	Ribulose bisphosphate carboxylase	**D**
11	Unidentified protein	**D**
15	Mitochondrial ATP synthase F1 beta subunit	**D**
20	High-CO_2-inducible periplasmic protein	**D**
23	Unidentified protein	**A**
24	Heat shock protein 90	-
25	Unidentified protein	-
27	Unidentified protein	-
31	Unidentified protein	-
32	Unidentified protein	-
33	Peridinin chlorophyll *a* binding protein	-
34	Unidentified protein	-
35	Unidentified protein	-
36	Hypothetical protein	-
37	Hypothetical protein	-
38	Mitochondrial ATP synthase F1 beta subunit	-
39	Mitochondrial ATP synthase F1 beta subunit	-
40	High-CO_2-inducible periplasmic protein	**D**
41	Ribulose bisphosphate carboxylase	-
45	Unidentified protein	-
46	Unidentified protein	-
48	Ribulose bisphosphate carboxylase	-
49	Light-harvesting protein	-

Figure 5

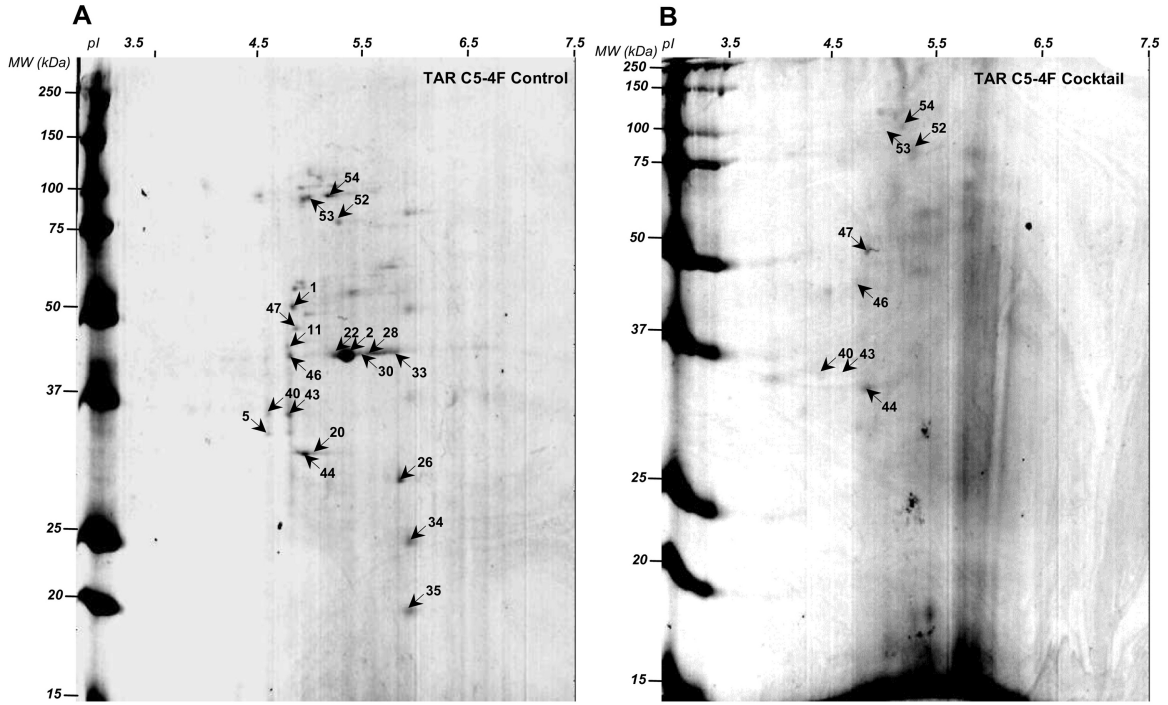

C

Spot n°	Protein name	Fold change
1	Unidentified protein	**-11.5***
2	Unidentified protein	**-16.7***
5	Unidentified protein	**D**
11	Unknown protein	**D**
20	Unidentified protein	**D**
22	High-CO_2-inducible periplasmic protein	**D**
26	Light-harvesting protein	**D**
28	Unidentified protein	**D**
30	High-CO_2-inducible periplasmic protein	**D**
33	High-CO_2-inducible periplasmic protein	**D**
34	ATP synthase CF1 beta chain	**D**
35	Light-harvesting polyprotein precursor	**D**
40	Ferredoxin-NADP(+) reductase	-
43	Ferredoxin-NADP(+) reductase	-
44	Chloroplast cytochrome f	-
46	Unidentified protein	-
47	ATP synthase CF1 beta chain	-
52	Unidentified protein	-
53	Unidentified protein	-
54	Unidentified protein	-

Figure 6